Article

Dynamic Response of $CoSb_2O_6$ Trirutile-Type Oxides in a CO_2 Atmosphere at Low-Temperatures

Alex Guillén-Bonilla [1],*, Verónica-María Rodríguez-Betancourtt [1], Martín Flores-Martínez [1], Oscar Blanco-Alonso [2], Juan Reyes-Gómez [3], Lorenzo Gildo-Ortiz [4] and Héctor Guillén-Bonilla [4]

[1] Materials Science Graduate School, CUCEI (Centro Universitario de Ciencias Exactas e Ingenierías), University of Guadalajara, Blvd. M. García Barragán 1421, Guadalajara, Jalisco 44410, Mexico; E-Mails: veronica.rodriguez@red.cucei.udg.mx (V.-M.R.-B.); doctorado.materiales@cucei.udg.mx (M.F.-M.)

[2] Physics Department, CUCEI (Centro Universitario de Ciencias Exactas e Ingenierías), University of Guadalajara, Blvd. M. García Barragán 1421, Guadalajara, Jalisco 44410, Mexico; E-Mail: oscar.blanco@cucei.udg.mx

[3] Faculty of Science, University of Colima, Bernal Díaz del Castillo 340, Colima, Colima 28045, Mexico; E-Mail: reyesgj@ucol.mx

[4] Faculty of Chemical Sciences, University of Colima, Km 9 Carretera Colima-Coquimatlán, Coquimatlán 28400, Colima, Mexico; E-Mails: lorenzo.gildo@gmail.com (L.G.-O.); hguillenbonilla@gmail.com (H.G.-B.)

* Author to whom correspondence should be addressed; E-Mail: alexguillenbonilla@gmail.com; Tel.: +52-33-38-36-45-00 (ext. 27941); Fax: +52-33-38-36-45-02.

Abstract: Experimental work on the synthesis of the $CoSb_2O_6$ oxide and its CO_2 sensing properties is presented here. The oxide was synthesized by a microwave-assisted colloidal method in presence of ethylenediamine after calcination at 600 °C. This $CoSb_2O_6$ oxide crystallized in a tetragonal structure with cell parameters $a = 4.6495$ and $c = 9.2763$ Å, and space group $P4_2/mnm$. To prove its physical, chemical and sensing properties, the oxide was subjected to a series of tests: Raman spectroscopy, Scanning Electron Microscopy (SEM) and impedance (Z) measurements. Microstructures, like columns, bars and hollow hemispheres, were observed. For the CO_2 sensing test, a thick film of $CoSb_2O_6$ was used, measuring the impedance variations on the presence of air/CO_2 flows (0.100 sccm/0.100 sccm) using AC (alternating current) signals in the frequency-range

0.1–100 kHz and low relative temperatures (250 and 300 °C). The CO_2 sensing results were quite good.

Keywords: sensing properties; $CoSb_2O_6$; trirutile; chemical synthesis

---

1. Introduction

Due to environmental concerns, the constant monitoring of the gases emitted to the atmosphere is highly important. Therefore, intense research on the gas-sensors area is carried out nowadays, especially regarding sensors based on semiconductor materials, like the oxides SnO_2, ZnO, TiO_2, WO_3, $LaFeO_3$ and $CoAl_2O_4$ [1–7]. Such materials show interesting sensing properties, remaining at the same time chemically stable in the presence of polluting gases. In recent years, oxides with a trirutile-type structure, like $CoSb_2O_6$ [8,9] and $ZnSb_2O_6$ [10,11], are being studied for gas-sensing applications with very good results. These results are mainly attributed to the nano-sized structure of the trirutile oxides, which therefore determines the best synthesis process (route) to produce them [9]. The ceramic method for the synthesis of oxides has been extensively used; however, this conventional process involves some disadvantages, for instance, it is necessary to heat the sample at elevated temperatures for a long time. Such treatment results in inhomogeneous materials, no control of the particle size and a decrease of the surface area. In order to overcome these problems, wet chemical routes can also be successfully employed, at relative low temperatures, yielding nanoparticles with unique microstructural features [12–14].

In addition, the response of a sensor in polluting gases atmospheres is strongly related to the chemical reactions occurring on the oxide surface; therefore, the microstructure determines the conversion efficiency of chemical interactions into electrical signals. So, it is very important to synthesize materials with optimal morphologies [1,15]. In this work we implemented a chemical synthesis route (the microwave-assisted colloidal method) to produce the $CoSb_2O_6$ oxide for gas sensing purposes. The employed synthesis route was found very convenient because a good stoichiometry control was possible, influencing positively on the microstructural characteristics of the oxide.

2. Experimental Section

2.1. Synthesis of Trirutile-Type CoSb₂O₆ Oxide

The trirutile-type structure $CoSb_2O_6$ oxide was synthesized based on the procedure described in [8,9]. However, in this work, these reagents were used: $SbCl_3$ (Sigma-Aldrich), $Co(NO_3)_2 \cdot 6H_2O$ (Mallinckrodt), 1 mL of ethylenediamine, and 5 mL of ethanol (Golden Bell). The resulting solution was evaporated by means of a microwave oven (JES769WK General Electric) at low power (180 W at 10–20 s intervals; the absorbed energy was calculated to be close to 85 kJ). The obtained precursor material was dried at 200 °C in static air for 8 h, then calcined in a muffle (Novatech) at 600 °C in static air for 6 h. In this process, a heating rate of 100 °C/h was employed.

2.2. Characterization of CoSb$_2$O$_6$ Powders

The calcined powders were analyzed by X-ray diffraction (XRD) at room temperature, using a D500 Siemens diffractometer (Siemens, Munich, Germany) with a Cu-Kα radiation (λ = 0.1518 nm). The 2θ scanning range was from 10° to 70° with a velocity of 1° min^{-1}. The powders were also analyzed by Raman spectroscopy (Renishaw, Inc, Schaumburg, IL, USA) using a 1000B microRaman Renishaw system, calibrated with a silicon semiconductor with its characteristic Raman peak at 520 cm^{-1}. The laser (excitation wavelength of 830 nm) was focused on the surface of the powders (spot size of approximately 20 μm) by means of a Leica optical microscope (DMLM; Leica microsystems, Deerfield, IL, USA) integrated to the microRaman system. The radiation energy on the sample was 4.5 mW 60 s. The morphology of the CoSb$_2$O$_6$ powders was analyzed by scanning electron microscopy (JEOL JSM-6390LV; Jeol, Inc., Dearborn, MI, USA).

The electrical characterization was made through dynamic tests of the impedance variation using a thick film made of oxide powders, which were set inside of a controlled tube-type furnace at temperatures of 250 and 300 °C. The impedance measurements were made by the two-tips technique using a computer controlled (with LabView 8.6, National Instruments) (Agilent 4263B device; Agilent Technologies, Inc, Santa Clara, CA, USA). The flow of the synthetic air/CO$_2$ gases was controlled by a MKS 647C controller (MKS Instruments, Inc, Andover, MA, USA).

3. Results and Discussion

3.1. X-Ray Diffraction Analysis

Figure 1 shows an X-ray diffraction pattern of the powders prepared by the above described method.

**Figure 1.** X-ray diffraction pattern of CoSb$_2$O$_6$ powders calcined at 600 °C in air.
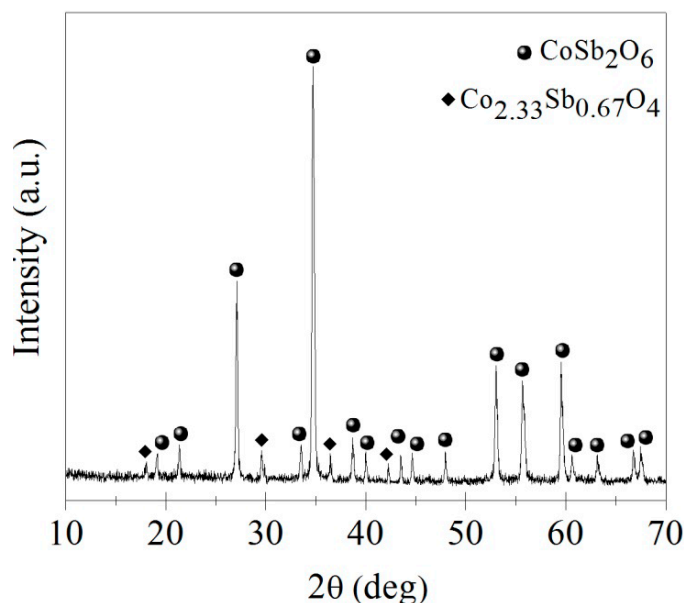
The diffractogram shows the presence of the main phase corresponding to $CoSb_2O_6$, which was identified using the file ICDD 203094. According to this card, the $CoSb_2O_6$ oxide crystallized in a tetragonal structure with cell parameters $a = 4.6495$ and $c = 9.2763$ Å, and space group $P4_2/mnm$ (136) [16], which indicates that the oxide belongs to the family of trirutile-type structures [17]. In addition, the width of the peaks in the diffraction spectra is an indication of crystals of nanometric size; the low noise level indicates that the sample possesses a high crystallinity [18]. The estimated crystal size according to the Scherrer equation [19] for the $CoSb_2O_6$ powders was around 41 nm. Furthermore, low intensity peaks identified through the ICDD 87234 file, reveal a secondary phase: $Co_{2.33}Sb_{0.67}O_4$ [9], localized on the angular positions $2\theta = 17.8°$, $2\theta = 29.5°$, $2\theta = 36.2°$, and $2\theta = 42°$.

Several other synthesis methods have been used for the preparation of oxides with trirutile-type structure. Larcher *et al.* [20] synthesized trirutile-type ASb_2O_6 materials (A = Ni, Cu, Co), following the solid-state reaction method, obtaining the structures at 800 °C. Michel *et al.* [21] obtained the $CoSb_2O_6$ oxide employing the solution-polymerization method at 700 °C. From the present work, and comparing with other studies, it can be stated that the obtention of the $CoSb_2O_6$ oxide is very feasible at temperatures significantly lower than those used by the authors above mentioned, by means of the synthesis route proposed here (the microwave-assisted colloidal method).
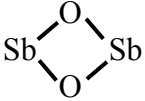
3.2. Raman Spectroscopy Analysis

The Raman analysis (Figure 2 and Table 1) shows the vibrations modes A_{1g}, B_{1g}, B_{2g} and E_g at the range 190–800 cm^{-1}. Band ν_1 has a mean intensity ~194 ± 3 cm^{-1} and is due to the vibrations of the crystalline network with A_{1g} symmetry. Band ν_2, at ~478 ± 3 cm^{-1}, is due to the deformation vibration of the Co-O bond, also with A_{1g} symmetry. Band ν_3, at ~518 ± 3 cm^{-1}, can be attributed to the combination of the stretching and coupling vibrations of the Sb-O bonds, with symmetry E_g. Band ν_4, at ~617 ± 3 cm^{-1}, is due to the asymmetric stretching vibration of the Sb-O bond, with symmetry E_g. Band ν_5, at ~641 ± 3 cm^{-1}, showing a high intensity, is due to the symmetric stretching vibration of the Sb-O bond, with E_g symmetry. These results are in agreement with [22] and [23], and support the correct characterization of the oxide.

Figure 2. Raman spectrum of $CoSb_2O_6$ powders calcined at 600 °C in air.
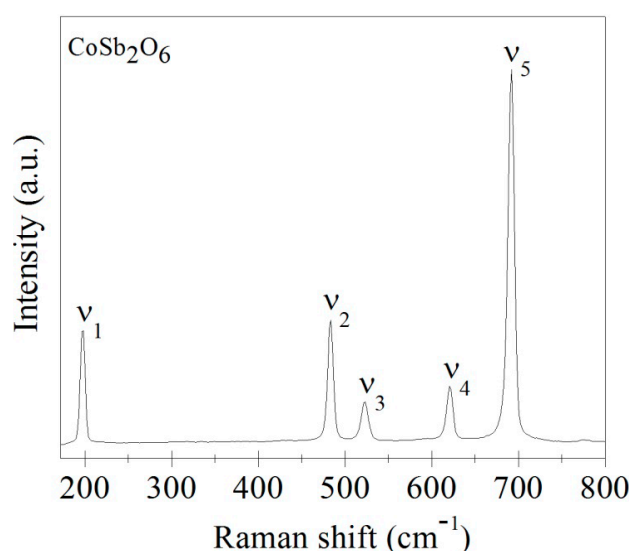
Table 1. Vibration modes of the CoSb$_2$O$_6$ oxide.

Mode	Raman Displacement (cm^{-1})	Symmetry	Vibration Type	Molecular Bond
v_1	~194 ± 3	A$_{1g}$	Crystalline network	
v_2	~478 ± 3	A$_{1g}$	Deformation	Co-O
v_3	~518 ± 3	E$_g$	Stretching and Coupling	Sb—O—Sb
v_4	~617 ± 3	E$_g$	Stretching (asymmetric)	Sb-O
v_5	~641 ± 3	E$_g$	Stretching (symmetric)	Sb-O

3.3. Scanning Electron Microscopy Analysis

Figure 3 shows photomicrographs of the CoSb$_2$O$_6$ oxide at several magnifications: (a) 350X, (b) 370X, and (c) 700X. The discerned particle shapes are rectangular micro-bars with sizes: base ~28.5 μm, length ~42 μm and height ~13 μm. Around these bars, some smaller structures in form of micro-rods, growing in different directions, are also discernible. The micro-rods growth, with an estimated diameter of ~2.7 μm, is attributed to the increasing of the temperature and the effects caused by the ethylenediamine. These micro-rods tend to aggregate to form a hollow hemisphere (see image b). The granulate surface of the micro-rods is probably due to the released gases from organic material during the thermal decomposition in the oxide's synthesis [24]. The size distribution of the micro-rods (also shown in Figure 3d) depicts a length range of 6–24 μm with a standard deviation of 3.4 μm and an average length of ~12.7 μm. The role of ethylenediamine in the formation of 1D structures of II–VI semiconductors, like nanorods and nanowires, has been discussed in previous works [25,26]. The ethylenediamine is incorporated first into the inorganic framework and then escapes from it to form particles of desired morphologies [26]. In this work, we found that the presence of ethylenediamine in the CoSb$_2$O$_6$ synthesis leads to the growth of micro-rods. In fact, we reported in a previous work [27] the obtention of trirutile-type MgSb$_2$O$_6$ with different morphologies, micro-rods and micro-plates among them, by the use of ethylenediamine.

Figure 3. SEM (scanning electron microscopy) images of CoSb$_2$O$_6$ powders at different magnifications: (**a**) 350X; (**b**) 370X; and (**c**) 700X; (**d**) length distribution of the micro-rods.
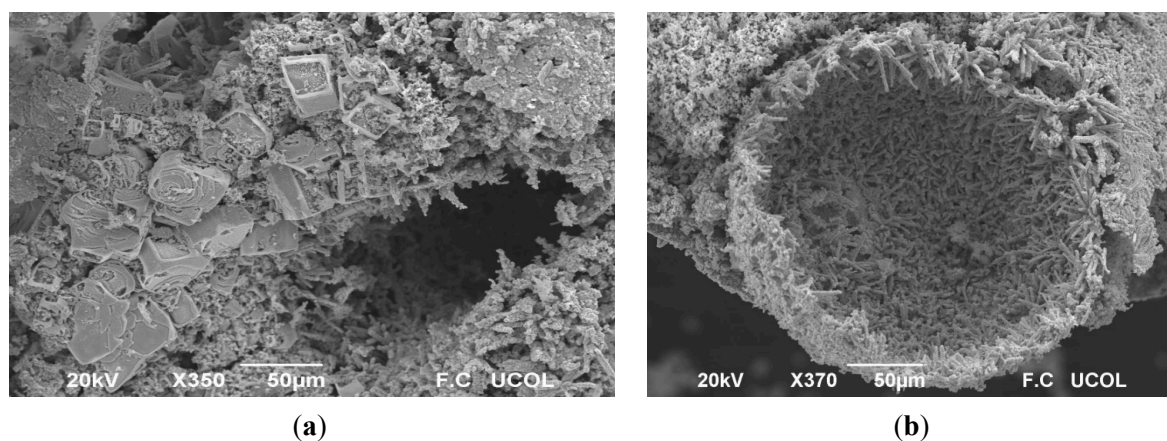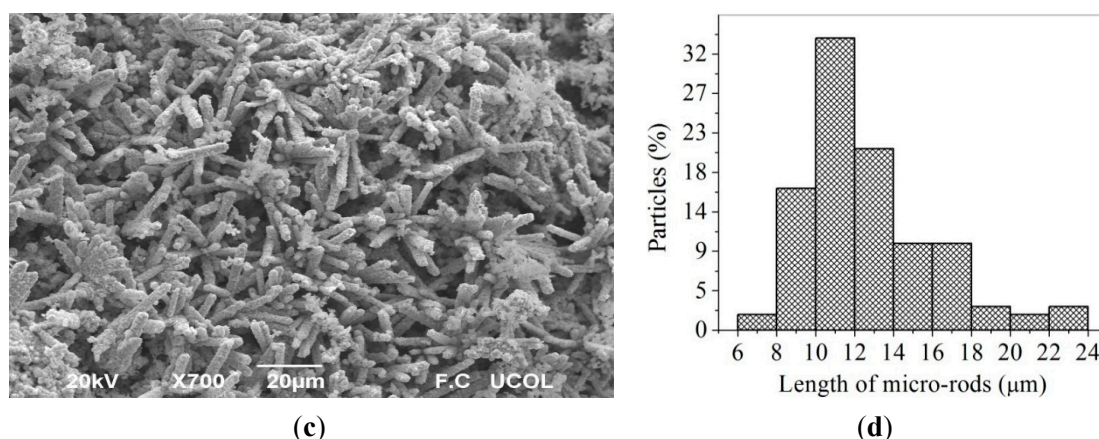

(**a**)

(**b**)

Figure 3. *Cont.*

(c)

(d)

On the other hand, the preparation of different inorganic compounds by means of colloidal routes has been widely studied by Matijevic [28]. Some authors report the obtention of morphologies similar to those here reported, which originate from the growth process of stable nuclei of the colloidal systems [28,29]. These morphologies are in agreement with the crystallization principles proposed by LaMer and Dinegar [9,24,27,30].

3.4. Impedance Measurements and Gas Sensing Properties

To test the gas sensing properties of the $CoSb_2O_6$ oxide, a thick film (thickness ~500 μm) was employed for measuring its impedance variation in presence of air/CO_2 flows (0.100 sccm/0.100 sccm). Experiments at four frequencies (AC (alternating current) signals) were conducted in this study: 0.1, 1, 10 and 100 kHz, and at two different temperatures, namely, 250 and 300 °C. The process to perform the dynamic response experiments consisted of three stages: (1) for each frequency and temperature, synthetic air was flowed over the film's surface during approximately 5 min in order to stabilize it; (2) a CO_2 flow was applied on the material, recording the impedance ($|Z|$) variations; (3) after one minute, synthetic air was flowed again over the thick film, returning the impedance $|Z|$ to the initial state. Figure 4 shows the dynamic tests results of the $CoSb_2O_6$ oxide at 250 °C, and Table 2 shows the calculated variations. In all four tests (0.1, 1, 10 and 100 kHz), the magnitude of the impedance ($|Z|$) changes in an alternating manner when the gas flow changes from air to CO_2. These results reveal that the material exhibits sensitivity and repeatability in CO_2 detection. In particular, at the 0.1 kHz frequency, the change of the magnitude $|Z|$ was ~3.23 kΩ on average (Figure 4a); while at the 1 kHz frequency, the recorded change was ~2.91 kΩ on average (Figure 4b). On the other hand, at the 10 kHz frequency, the magnitude of the impedance changes ~2.43 kΩ on average (Figure 4c); however, using a high frequency of 100 kHz, the magnitude of the impedance is reduced to an average value of ~1.71 kΩ (Figure 4d).

In addition, Figure 4 shows the fast response and recovery times recorded during the exposure to the CO_2 gas at 250 °C. The response times, measured at 90% of the full response, were 22.38, 21.56, 20.32 and 18.19 s at the frequencies 0.1, 1, 10 and 100 kHz, respectively, while the recorded recovery times were 21.36, 20.06, 19.06 and 17.95 s at the same frequencies, respectively (See Table 2). From

these results, $CoSb_2O_6$ thick films respond faster and with a shorter recovery time at the higher frequency (100 kHz); however, upon increasing the frequency, smaller $|Z|$ values were registered.

Figure 4. Dynamic response of the $CoSb_2O_6$ oxide subjected to CO_2 flows at 250 °C and different frequencies: (**a**) 0.1 kHz; (**b**) 1 kHz; (**c**) 10 kHz; and (**d**) 100 kHz.
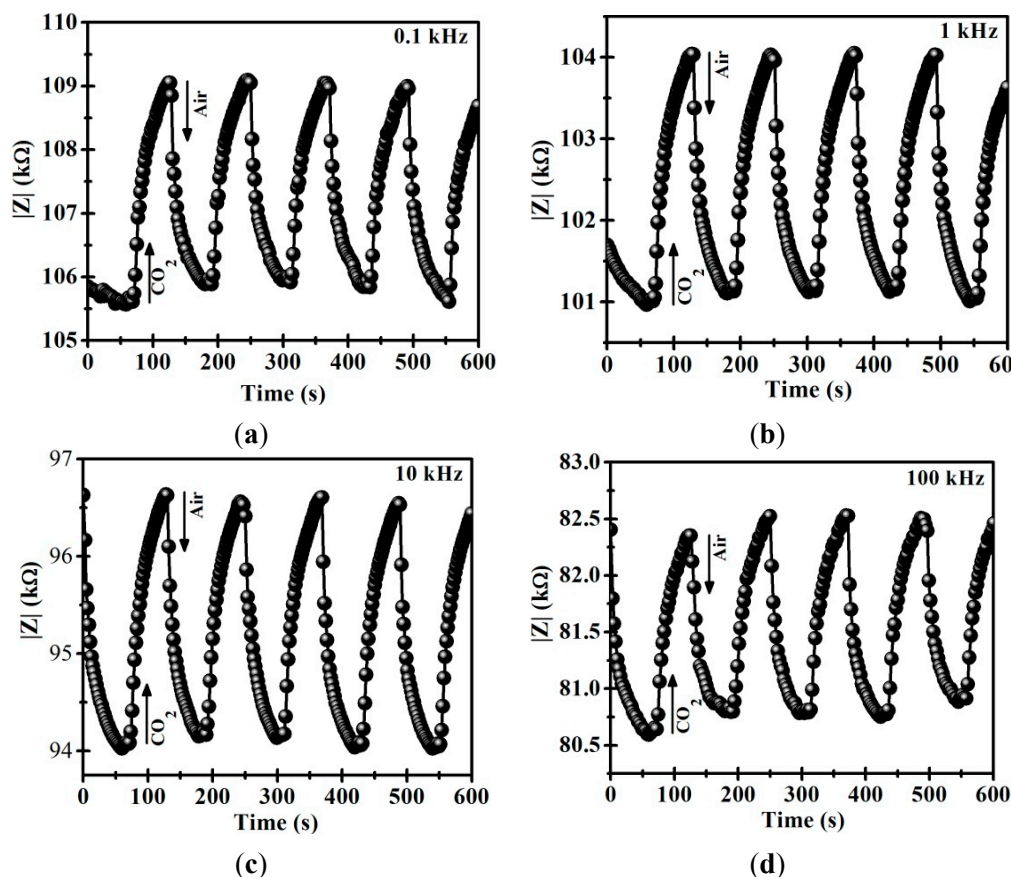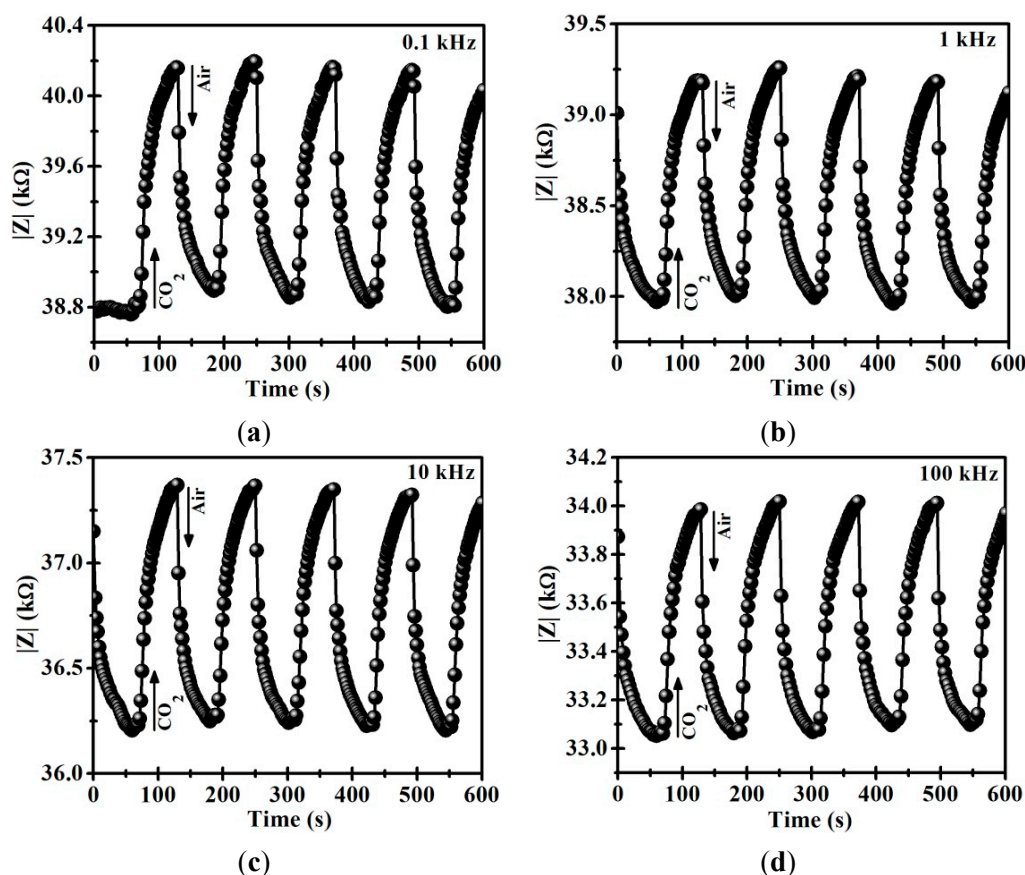

Table 2. Variations of the impedance measurement at 250 °C.

Frequency (kHz)	Mean Impedance (kΩ)	Response Time (s)	Recovering Time (s)
0.1	3.23	22.38	21.36
1	2.91	21.56	20.06
10	2.43	20.32	19.06
100	1.71	18.19	17.95

Figure 5 shows the results of the dynamic tests on the $CoSb_2O_6$ oxide at 300 °C with the same frequencies and gases flows, and the calculated variations are shown in Table 3. Similar tendencies to those shown in Figure 4 were recorded. However, at 300 °C, the changes of the magnitude $|Z|$ were ~1.29, ~1.18, ~1.09 and ~0.921 kΩ, at the frequencies 0.1, 1, 10 and 100 kHz, respectively. In addition, the response and recovery times were reduced to values less than 20 s due to the effect of the temperature. In this case, the response times were 17.32, 16.30, 15.00 and 14.18 s, while the recovery times were 16.18, 15.00, 13.93 and 13.00 s at the same frequencies, respectively (see Table 3). Clearly, at higher temperatures and frequencies applied, the $CoSb_2O_6$ sensor exhibits faster response and shorter recovery times.

Figure 5. Dynamic response of the $CoSb_2O_6$ oxide subjected to CO_2 flows at 300 °C and different frequencies: (**a**) 0.1 kHz; (**b**) 1 kHz; (**c**) 10 kHz; and (**d**) 100 kHz.

(**a**)   (**b**)

(**c**)   (**d**)

Table 3. Variations of the impedance measurement at 300 °C.

| Frequency (kHz)	Mean Impedance (kΩ)	Response Time (s)	Recovering Time (s)
0.1	1.29	17.32	16.18
1	1.18	16.30	15.00
10	1.09	15.00	13.93
100	0.921	14.18	13.00

To discern the effects of frequency and temperature on the $CoSb_2O_6$ ability to detect air/CO_2, Figure 6 shows graphically the above mentioned variations. Clearly, increasing the frequency and the temperature, the impedance drops considerably, which is a characteristic of semiconductor materials. At 250 °C, the average $|Z|$ is 2.52 kΩ and at 300 °C, it is 1.12 kΩ. The oxide therefore behaves like a low-pass filter and can be modeled as a parallel RC circuit (see Figure 7). This circuit is made up of the alternating current (AC) source, a resistance (R) and a capacitor (C) [8]. In addition, the behavior of the dynamic response obtained at 250 and 300 °C can be reproducible. This suggests that this material can reliably be applied as a gas sensor under air/CO_2 flows [31].

Figure 6. Impedance |Z| *vs.* frequency tests of the CoSb$_2$O$_6$ oxide at (**a**) 250 °C and (**b**) 300 °C with air/CO$_2$ flows.

(**a**)   (**b**)
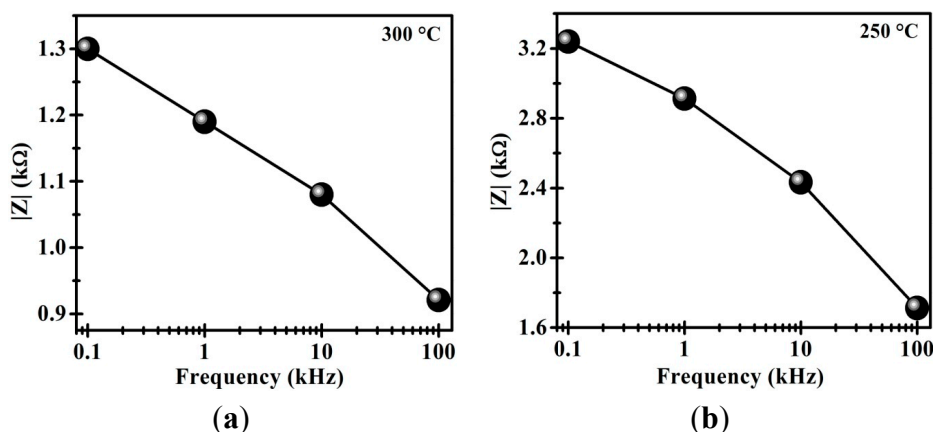
Figure 7. Equivalent RC parallel circuit for the CoSb$_2$O$_6$ sensor.
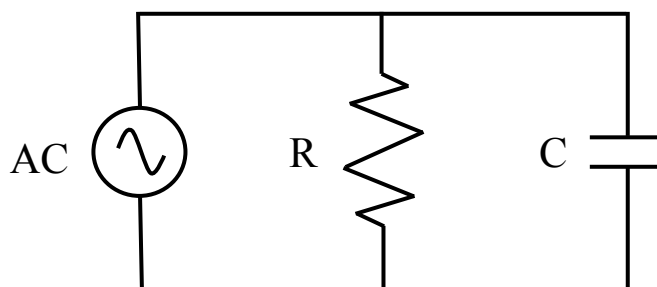
Comparing the results of Figures 4 and 5 with those reported in previous works corresponding to the CoSb$_2$O$_6$ oxide, a better performance as gas sensor was obtained in the present work. For example, nanostructured CoSb$_2$O$_6$ microspheres have been synthesized employing a non-aqueous method in presence of n-dodecylamine [9]. These CoSb$_2$O$_6$ microspheres were sensitive to detect 400 ppm of CO$_2$ at 400 °C with a response time of 130 s and a recovery time of 22 s. Also, the variation in electrical resistance recorded was 130 Ω. In addition, the dynamic response of CoSb$_2$O$_6$ prepared by solution-polymerization method has been reported [21]. In this paper, a CO$_2$ flow (100 cm^3/min) produces an increase in electrical resistance of 900 Ω in 3 min (410 °C). However, the CoSb$_2$O$_6$ oxide synthesized in this work exhibits good sensing properties at lower temperatures (250 and 300 °C) to those reported in the previous works. Additionally, a faster response, shorter recovery times, better repeatability and larger impedance changes were obtained. This gas response can be attributed to the microstructure found in this work, and its nanocrystalline nature.

Moreover, from Figures 4 and 5 the rise of |Z| during the flow of CO$_2$ indicates a p-type semiconductor [31,32]. In general, the gas-sensing mechanism in semiconductor materials is based on the electric resistance change (conductance) produced by the electron transfer occurring during the chemical adsorption [32]. In the presence of a gas, such as the one used in this study (CO$_2$), electrons are provided to the oxide surface and they combine with holes. Therefore, the concentration of electrical charge carriers (holes) is reduced and the magnitude |Z| increases. The process of CO$_2$ adsorption on metal oxide surfaces can involve the formation of several carbon species, such as

bicarbonate and carbonates [33]. These carbon species are removed when air is injected. Then, the magnitude $|Z|$ reached its original value.

Depending on the type of the semiconductor, the concentration of the charge carriers on the surface can be increased or decreased [34]. The thickness of the charged L_S outer layer can be defined as [34]:

$$L_S = L_D \sqrt{\left|\frac{eV_S^2}{kT}\right|} \tag{1}$$

where L_D is the Debye length, e is the charge of the electron, V_S is the potential of the surface, k is the Boltzmann constant, and T is the temperature. Usually, the L_S values are between 1 and 100 nm [34].

According to some authors, the charged outer layer mainly depends on the gas pressure and the gas concentrations. These results of the changing resistance value and the conductivity variation of the semiconductor can be consulted in [35]. Due to this, the conductivity strongly depends on the size of the crystal (D), thus giving rise to three possible scenarios [36]:

(1) If $D \gg 2L_S$, the conductivity is limited by the Schottky barrier at the particle border; thus, the gas detection does not depend on the crystal size (D),

(2) If $D = 2L_S$, the conductivity and the gas sensing depend on necks formed by the crystals, and

(3) If $D < 2L_S$, the conductivity depends on the crystal size [36,37]. Based on these three scenarios, it can be said that the smaller the size of the particle during its synthesis, the greater the surface area obtained and, therefore, a better gas adsorption [34].

In addition, the good electric response of the $CoSb_2O_6$ under a controlled air/CO_2 flow can be to a great extent explained by the presence of microstructures obtained during the process of synthesis.

4. Conclusions

Desirable trirutile-type $CoSb_2O_6$ structures for gas-sensing applications, like micro-rods and micro-bars, were successfully prepared by a wet-chemical synthesis route at relative low temperatures. The results of this work, regarding the sensing properties of the synthesized material, show that at different frequencies, the dynamic response improves under air/CO_2 flows. The $CoSb_2O_6$ thick films respond faster and with a shorter recovery time at higher temperatures and frequencies (100 kHz and 300 °C). Also, the results indicated that increasing the frequency, smaller $|Z|$ values were obtained. The uniformity of the dynamic tests reflects the good impedance response during the adsorption of the CO_2. According to this, the $CoSb_2O_6$ oxide is a strong candidate to be applied as an environmental gas sensor, especially when synthesized by our proposed method.

Author Contributions

Verónica-María Rodríguez-Betancourtt was the supervisor of the PhD work of the author (Alex Guillén-Bonilla), from which this study results and contributed with work on the Raman spectroscopy analysis and the writing of this article; Martín Flores-Martínez contributed with work on the XRD analysis; Oscar Blanco-Alonso contributed with work on the gas-sensing tests; Juan Reyes-Gómez contributed with work on the SEM; Lorenzo Gildo-Ortiz contributed on observations, recommendations, discussion and a critical review of the manuscript; Héctor Guillén-Bonilla contributed with work on the synthesis method and the writing of this article. All authors read and approved the final manuscript.

Conflicts of Interest

The authors declare no conflict of interest.

References

1. Wang, C.; Yin, L.; Zhang, L.; Xiang, D.; Gao, R. Metal oxide gas sensors: Sensitivity and influencing factors. *Sensors* **2010**, *10*, 2088–2106.
2. Gómez-Pozos, H.; González-Vidal, J.L.; Torres, G.A.; Olvera, M.L.; Castañeda, L. Physical characterization and effect of effective surface area on the sensing properties of tin dioxide thin solid films in a propane atmosphere. *Sensors* **2014**, *14*, 403–415.
3. Gómez-Pozos, H.; González-Vidal, J.L.; Torres, G.A.; Rodríguez-Baez, J.; Maldonado, A.; Olvera, M.L.; Acosta, D.R.; Avendaño-Alejo, M.; Castañeda, L. Chromium and ruthenium-doped zinc oxide thin films for propane sensing applications. *Sensors* **2013**, *13*, 3432–3444.
4. Zhao, J.; Liu, Y.; Li, X.; Lu, G.; You, L.; Liang, X.; Liu, F.; Zhang, T.; Du, Y. Highly sensitive humidity sensor based on high surface area mesoporous $LaFeO_3$ prepared by a nanocasting route. *Sens. Actuators B Chem.* **2013**, *181*, 802–809.
5. Li, Z.; Ding, D.; Liu, Q.; Ning, C. Hydrogen sensing with Ni-doped TiO_2 nanotubes. *Sensors* **2013**, *13*, 8393–8402.
6. Gui, Y.; Yuan, J.; Wang, W.; Zhao, J.; Tian, J.; Xie, B. Facile solvothermal synthesis and gas sensitivity of graphene/WO_3 nanocomposites. *Materials* **2014**, *7*, 4587–4600.
7. Michel, C.R. CO and CO_2 gas sensing properties of mesoporous $CoAl_2O_4$. *Sens. Actuators B Chem.* **2010**, *147*, 635–641.
8. Michel, C.R.; Martínez, A.H.; Morán, J.P. Effect of the frequency on the gas sensing response of $CoSb_2O_6$ prepared by a colloidal method. *Sens. Actuators B Chem.* **2009**, *140*, 149–154.
9. Michel, C.R.; Guillén, H.; Martínez, A.H.; Morán, J.P. Synthesis and gas sensing properties of $CoSb_2O_6$ microspheres. *Sens. Actuators B Chem.* **2009**, *143*, 278–285.
10. Tamaki, J.; Yamada, Y.; Yamamoto, Y.; Matsuoka, M.; Ota, I. Sensing properties to dilute hydrogen sulfide of $ZnSb_2O_6$ thick-film prepared by dip-coating method. *Sens. Actuators B Chem.* **2000**, *66*, 70–73.
11. Zhu, B.L.; Xie, C.S.; Wang, A.H.; Zeng, D.W.; Hu, M.L.; Wang, W.Y. Electrical conductivity and gas sensitivity of Zn-Sb-O thick films. *Mater. Res. Bull.* **2004**, *39*, 409–415.

12. Jung, W.Y.; Hong, S.S. Synthesis of $LaCoO_3$ nanoparticles by microwave process and their photocatalytic activity under visible light irradiation. *J. Ind. Eng. Chem.* **2013**, *19*, 157–160.

13. Sompech, S.; Srion, A.; Nuntiya, A. The effect of ultrasonic treatment on the particle size and specific surface area of $LaCoO_3$. *Procedia Eng.* **2012**, *32*, 1012–1018.

14. Khun, K.; Ibupoto, Z.H.; AlSalhi, M.S.; Atif, M.; Ansari, A.A.; Willander, M. Fabrication of well-aligned ZnO nanorods using a composite seed layer of ZnO nanoparticles and chitosan polymer. *Materials* **2013**, *6*, 4361–4374.

15. Mei, L.; Deng, J.; Yin, X.; Zhang, M.; Li, Q.; Zhang, E.; Xu, Z.; Chen, L.; Wang, T. Ultrasensitive ethanol sensor based on 3D aloe-like SnO_2. *Sens. Actuators B Chem.* **2012**, *166*, 7–11.

16. Jamal, A.; Rahman, M.M.; Khan, S.B.; Faisal, M.; Akhtar, K.; Rub, M.A.; Asiri, A.M.; Al-Youbi, A.O. Cobalt doped antimony oxide nano-particles based chemical sensor and photo-catalyst for environmental pollutants. *Appl. Surf. Sci.* **2012**, *261*, 52–58.

17. Mizoguchi, H.; Woodward, P.M. Electronic structure studies of main group oxides possessing edge-sharing octahedra: implications for the design of transparent conducting oxides. *Chem. Mater.* **2004**, *16*, 5233–5248.

18. Delgado, E.; Michel, C.R. CO_2 and O_2 sensing behavior of nanostructured barium-doped $SmCoO_3$. *Mater. Lett.* **2006**, *60*, 1613–1616.

19. Holzwarth, U.; Gibson, N. The Scherrer equation versus the 'Debye Scherrer equation'. *Nat. Nanotechnol.* **2011**, *6*, doi:10.1038/nnano.2011.145.

20. Larcher, D.; Prakash, A.S.; Laffont, L.; Womens, M.; Jumas, J.C.; Olivier-Fourcade, J.; Hedge, M.S.; Tarascon, J.-M.M. Reactivity of antimony oxides and MSb_2O_6 (M = Cu, Ni, Co), trirutile-type phases with metallic lithium. *J. Electrochem. Soc.* **2006**, *153*, A1778–A1787.

21. Michel, C.R.; Martínez, A.H.; Jiménez, S. Gas sensing response of nanostructured trirutile-type $CoSb_2O_6$ synthesized by solution-polymerization method. *Sens. Actuators B Chem.* **2008**, *132*, 45–51.

22. Haeuseler, H. Infrared and Raman spectra and normal coordinate calculations on trirutile-type compounds. *Spectrochim. Acta Part A Mol. Spectrosc.* **1981**, *37*, 487–495.

23. Husson, E.; Repelin, Y.; Brusset, H.; Cerez, A. Spectres de vibration et calcul du champ de force des antimoniates et des tantalates de structure trirutile. *Spectrochim. Acta Part A Mol. Spectrosc.* **1979**, *35*, 1171–1187. (in French)

24. Gildo-Ortiz, L.; Guillén-Bonilla, H.; Santoyo-Salazar, J.; Olvera, M.L.; Karthik, T.V.K.; Campos-González, E.; Reyes-Gómez, J. Low-temperature synthesis and gas sensitivity of perovskite-type $LaCoO_3$ nanoparticles. *J. Nanomater.* **2014**, *2014*, doi: org/10.1155/2014/164380.

25. Deng, Z.-X.; Wang, C.; Sun, X.-M.; Li, Y.D. Structure-directing coordination template effect of ethylenediamine in formations of ZnS and ZnSe nanocrystallites via solvothermal route. *Inorg. Chem.* **2002**, *41*, 869–873.

26. Wang, X.; Li, Y. Solution-based synthetic strategies for 1-D nanostructures. *Inorg. Chem.* **2006**, *45*, 7522–7534.

27. Guillén, H.; Reyes, J.; Guillén, A.; Pozas, D.; Guillén, J.T.; Gildo, L.; Flores, M. Synthesis and characterization of $MgSb_2O_6$ trirutile-type in low presence concentrations of ethylenediamine. *J. Chem. Chem. Eng.* **2013**, *7*, 395–401.

28. Matijevic, E. Uniform inorganic colloid dispersions. Achievements and challenges. *Langmuir* **1994**, *10*, 8–16.
29. Matijevic, E. Monodispersed colloids: Art and science. *Langmuir* **1986**, *2*, 12–20.
30. LaMer, V.K.; Dinegar, R.H. Theory, production and mechanism of formation of monodispersed hydrosols. *J. Am. Chem. Soc.* **1950**, *72*, 4847–4854.
31. Michel, C.R.; Martínez-Preciado, A.M.; Morán-Lázaro, J.P.; Guillén-Bonilla, H. CO_2 detection in nanostructured $CoSb_2O_6$ prepared by a non-aqueous colloidal method. *ECS Trans.* **2010**, *25*, 49–51.
32. Moseley, P.T. Materials selection for semiconductor gas sensors. *Sens. Actuators B Chem.* **1992**, *6*, 149–156.
33. Tsuji, H.; Okamura-Yoshida, A.; Shishido, T.; Hattori, H. Dynamic behavior of carbonate species on metal oxide surface: Oxygen scrambling between adsorbed carbon dioxide and oxide surface. *Langmuir* **2003**, *19*, 8793–8800.
34. Bochenkov, V.E.; Sergeev, G.B. Preparation and chemiresistive properties of nanostructured materials. *Adv. Colloid Interface Sci.* **2005**, *116*, 245–254.
35. Michel, C.R.; Delgado, E.; Martínez, A.H. Evidence of improvement in gas sensing properties of nanostructured bismuth cobaltite prepared by solution-polymerization method. *Sens. Actuators B Chem.* **2007**, *125*, 389–395.
36. Yamazoe, N. New approaches for improving semiconductor gas sensors. *Sens. Actuators B Chem.* **1991**, *5*, 7–19.
37. Yamazoe, N. Toward innovations of gas sensor technology. *Sens. Actuators B Chem.* **2005**, *108*, 2–14.